Report of Investigations 8828

Vertical Magnetic Noise in the Voice Frequency Band Within and Above Coal Mines

By John Durkin

UNITED STATES DEPARTMENT OF THE INTERIOR
William P. Clark, Secretary

BUREAU OF MINES
Robert C. Horton, Director

Library of Congress Cataloging in Publication Data:

Durkin, John

Vertical magnetic noise in the voice frequency band within and above coal mines.

(Report of investigations ; 8828)

Bibliography: p. 21-22.

Supt. of Docs. no.: I 28.23:8828.

1. Coal mines and mining—Communication systems. 2. Electromagnetic noise. 3. Voice frequency. I. Title. II. Series: Report of investigations (United States. Bureau of Mines) ; 8828.

TN23.U43 [TN344] 622s [622] 83-600164

CONTENTS

	Page
Abstract	1
Introduction	2
EM atmospheric noise	2
Noise source	2
Earth-ionosphere waveguide	5
Prior atmospheric noise measurements	8
Surface vertical magnetic noise	9
Underground vertical magnetic noise	11
EM vertical magnetic noise field tests	12
Noise measuring instrumentation	12
Noise data	14
Data analysis	16
Summary	21
References	21
Appendix A.--Abbreviations and symbols used in this report	23
Appendix B.--Instrumentation noise	24
Appendix C.--Mine identification	27

ILLUSTRATIONS

1.	Vertical electric dipole on surface of a perfectly conducting earth	3
2.	Expected vertical-moment time variation for main cloud-to-ground discharge	4
3.	Expected frequency spectrum of radiation component of electric field	5
4.	Directionality diagram of average number of atmospherics occurring in 1 day	5
5.	Propagation attenuation coefficient of earth-ionosphere waveguide	7
6.	Relative vertical electric noise field spectrum	8
7.	Typical vertical electric field noise measurements	9
8.	Coordinate system and earth conductivity model	10
9.	Geometry of homogeneous half-space earth model with thin conducting sheet	12
10.	Field test recording instrumentation	13
11.	Playback instrumentation	14
12.	Surface and underground mean vertical magnetic noise values from noise data	17
13.	Regression results for surface and underground vertical magnetic noise versus frequency	19
B-1.	Noise-equivalent model of receiver	24

TABLES

1.	Surface and underground vertical magnetic noise values obtained at different sites	15
2.	Surface and underground vertical magnetic noise mean and standard deviation values	16
3.	Regression results for vertical magnetic noise	18
4.	Expected vertical magnetic noise values for one-third octaves	20
C-1.	Mines from which magnetic noise measurements were obtained	27

UNIT OF MEASURE ABBREVIATIONS USED IN THIS REPORT

A	ampere	m	meter
A m	ampere meter	m^2	square meter
A/m	ampere per meter	µA	microampere
dB	decibel	MHz	megahertz
dB/Mm	decibel per megameter	Mm	megameter
F/m	farad per meter	m/s	meter per second
ft	foot	µs	microsecond
h	hour	µV m	microvolt meter
Hz	hertz	pct	percent
in	inch	Ω	ohm
J/K	joule per kelvin	rad/s	radian per second
K	kelvin	s	second
kHz	kilohertz	V/m	volt per meter
km	kilometer		

VERTICAL MAGNETIC NOISE IN THE VOICE FREQUENCY BAND WITHIN AND ABOVE COAL MINES

By John Durkin [1]

ABSTRACT

Information on vertical magnetic noise in the voice frequency band, both within and above coal mines, is needed for the evaluation of through-the-earth baseband electromagnetic communications at mines where horizontal loop antennas are used. This report discusses the theory of the source of electromagnetic noise, the propagation of this noise to an observation point above a mine, and its interaction with the local earth conductivity structure, which gives rise to vertical magnetic noise. The relationship of surface noise to underground noise is also discussed.

Bureau of Mines investigators made surface and underground vertical magnetic noise measurements at a number of coal mines located throughout the United States. These data were modeled through regression analysis to characterize expected noise levels. The results are presented, including results in one-third octaves for use in evaluating the expected performance of through-the-earth communication systems by articulation-index studies.

[1]Electrical engineer, Pittsburgh Research Center, Bureau of Mines, Pittsburgh, PA.

INTRODUCTION

The performance of through-the-earth (TTE) communication systems is limited by noise, which degrades the intelligibility of voice reception and causes errors in digital data communication. Noise is an additive disturbance whose effects can be reduced by increasing the signal power, by proper signal design, or by signal processing. TTE communication systems are affected by three basic types of noise: instrumentation, atmospheric, and manmade. Thermal noise, generated by resistance in the antenna and front-end circuits, determines the receiver's ultimate sensitivity. (A discussion of instrumentation noise and its influence on electromagnetic (EM) noise measurements when using an air-core loop antenna is given in appendix B.) Atmospheric noise is a natural occurrence caused by lightning strokes which radiate EM impulses that propagate great distances. Manmade noise is usually caused by power lines and can severely limit the performance of a TTE communication system.

Instrumentation, atmospheric, and manmade noise all have different characteristics. The average power of thermal noise is fairly constant, whereas atmospheric and manmade noise may vary considerably with time and frequency. The probability density distribution of thermal noise is typically Gaussian, whereas atmospheric noise contains intermittent impulses superimposed on a Gaussian noise background. The characteristics of manmade noise vary considerably, but the observed spectrum usually contains several discrete frequency components with varying amplitudes. Manmade noise is a continuous-wave (CW) interference that generally occurs at 60 Hz and at various harmonics of 60 Hz extending to several kilohertz.

In order to design a communication system and predict its performance, several basic pieces of information about existing noise must be known. The most important aspects are the level of and variation in noise amplitude in the short and long term. For example, the amplitude of atmospheric noise varies both hourly and seasonally. However, before amplitude measurements are considered, the type of measurement that will extract significant and useful information from the noise phenomena must be determined. For this purpose, the frequency of interest and the associated bandwidth of the communication system must be known. Where measurement of broadband noise is required for predicting communication system performance, the root-mean-square (RMS) noise value is the most useful single measurement. This has long been recognized, as shown by the International Radio Consultative Committee (CCIR) (8).[2]

Amplitude variation over the frequency band of interest also presents valuable information. Depending upon the nature of its application, amplitude variation information may be in the form of spectral density or it may be broken into a number of bands such as one-third octaves. One value of spectral density information is that manmade noise contributions can be easily discerned. Also, since TTE communications may be two way, both uplink and downlink, information on the expected levels and relationships of both surface and underground noise must be obtained; and spectral density data provides this information.

EM ATMOSPHERIC NOISE

NOISE SOURCE

The primary source of EM noise in the extremely low frequency (ELF) through the very low frequency (VLF) range can be attributed to lightning discharges from both local thunderstorm activity and distant storms from which the EM noise propagates in the earth-ionosphere waveguide.

[2]Underlined numbers in parentheses refer to items in the list of references preceding the appendixes.

A lightning stroke consists of three main sections--the predischarge, main discharge, and slow tail--each of which produces energy in a different frequency range (15). The predischarge consists of a series of leaders of very short duration and produces energy in the 30 to 100 kHz range. This is followed by the main discharge, which lasts approximately 100 μs and produces energy in the 30 to 1,000 kHz frequency range. The main discharge is followed by the slow tail, which lasts up to 1/2 s and produces energy below 1,000 Hz.

At a distance (d) from a lightning stroke, the received noise record (N) is controlled both by the source waveform (S) and the characteristics of the channel (W) in which the noise propagates. In general, the spectral component (f) of the noise can be written as

$$N(f) = S(f) \cdot W(d,f). \qquad (1)$$

The signal generated by a lightning stroke can be considered to be produced by many dipole radiators of different dimensions at the source location. Wait (20) has characterized the lightning stroke as a single vertical electric dipole source. A vertical electric dipole on the surface of a perfectly conducting flat earth (fig. 1) produces both electric and magnetic fields. If the current along the dipole of effective height (h_e) is assumed to be uniform, the resulting RMS electric and magnetic fields are

$$E_z = \frac{Ih_e}{2\pi\varepsilon_0}\left(\frac{1}{\omega d^3} + \frac{i}{cd^2} - \frac{\omega}{c^2 d}\right) \qquad (2)$$

and

$$H_\phi = \frac{Ih_e}{2\pi}\left(\frac{i}{d^2} - \frac{\omega}{cd}\right), \qquad (3)$$

where E_z = RMS vertical electric field, V/m,

H_ϕ = RMS tangential magnetic field, A/m,

ε_0 = permittivity of free space, F/m,

I = antenna current, A,

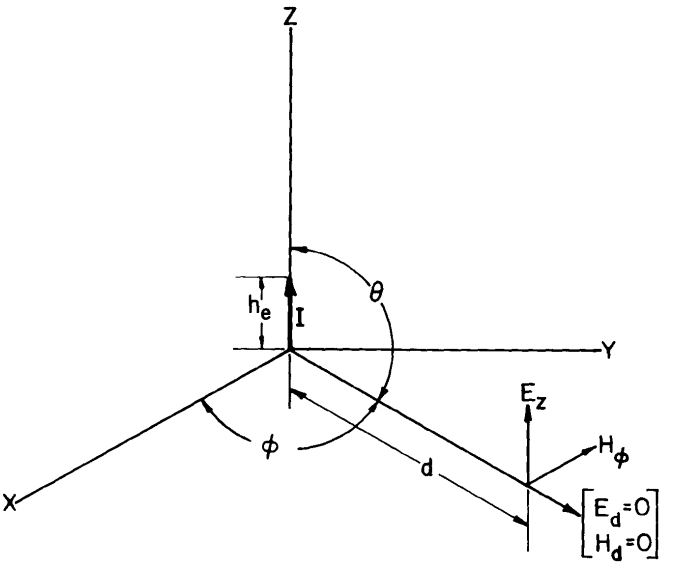

FIGURE 1. - Vertical electric dipole on surface of a perfectly conducting earth. (See text and appendix A for identification of symbols.)

d = distance between observation point and antenna (and is assumed to be large compared to h_e),

c = velocity of light, m/s,

ω = frequency, rad/s,

and i = imaginary number.

The term in equation 2 associated with d^3 is the electrostatic field. An electrostatic field is present if the dipole consists only of separated stationary charges. This can be seen from equation 2, where the electrostatic term is proportional to the time integral of current, i.e., $q \cdot h_e$, where q = charge. The induction field is directly proportional to $I \cdot h_e$. The radiation term (i.e., $dI/dt \cdot h_e$, where t = time), results only from a change in current and is directly proportional to the current differential.

During an actual lightning stroke, both I and h_e are functions of time. The current flow in the dipole source creates a time-variable charge moment of

$$M(t) = I(t) \cdot h_e(t), \qquad (4)$$

where M(t) is the changing vertical electric moment in amperes per meter.

In most atomspheric noise studies, the radiation field is of most interest. The electric and magnetic radiation fields can be written in terms of the charge moment as

$$E_z(t) = -\frac{1}{2\pi\varepsilon_0}\,\frac{dM(t)/dt}{c^2 d} \qquad (5)$$

and

$$H_\phi(t) = \frac{1}{2\pi}\,\frac{dM(t)/dt}{cd}. \qquad (6)$$

E_z/H_ϕ = 377 Ω, the free-space wave impedance (η). When equations 5 and 6 are used to determine variations in electric and magnetic fields, the retarded values of M(t) at time (t - d/c) should be used in order to account for propagation delay. If the radiation field terms are to be measured, the observation point must be far enough from the source that the electrostatic and induction fields will be negligible. At $d = \lambda/2\pi$, where λ = wavelength, the induction and radiation terms are equal. Beyond one wavelength, both the electric and magnetic fields decay as 1/d. Thus, beyond 50 km, the far field term dominates for frequencies exceeding 1 kHz.

Based on the assumptions presented above, the magnitudes of the fields can be expected to exhibit an inverse distance dependence. This has been shown experimentally by Bradley (7) for distances from 20 to 200 km. At very short distances (d < 20 km), d is comparable to the length of the discharge, which then does not behave as a dipole source. At great distances (d > 200 km), the ionospheric influence becomes appreciable.

The heights of discharge paths differ appreciably, giving rise to large variability in the electric moment. Watt (23) shows typical time behavior curves for the main cloud-to-ground discharge of the effective vertical moment and its differential and integral forms. These curves

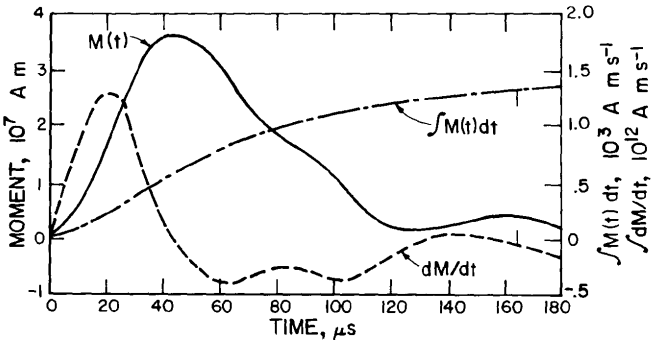

FIGURE 2. - Expected vertical-moment time variation for main cloud-to-ground discharge (23).

are shown in figure 2. The source radiation spectrum can be determined by obtaining the Fourier transformation of the dM/dt curve from

$$S(\omega) = \int_0^\tau dM/dt \cdot \exp^{-i\omega t}\, dt, \qquad (7)$$

where τ is the duration of the waveform. Watt (23) has calculated this Fourier transformation and the results are shown in figure 3. Since dM/dt may vary appreciably, the actual spectrum of any particular cloud-to-ground discharge may also vary appreciably. However, the spectrum shown in figure 3 can be considered to be the expected noise source spectrum for S from equation 1.

The direction of arrival of distant storms (the source of most EM noise energy) is also discussed by Watt (23). Figure 4 shows the average number of atmospherics occurring in a 24-h period, based on data gathered over 4 days in October and plotted as a function of direction of arrival. Most noise sources are located in one of three azimuth sectors; these are Africa, South America, and Indonesia. At given observation point, the amplitude of the noise and the direction of its arrival are found to coincide with the time of day of the buildup of thunderstorm activity in one of these sectors. Local storms, which are finite in number, produce an impulsive form at the observation point.

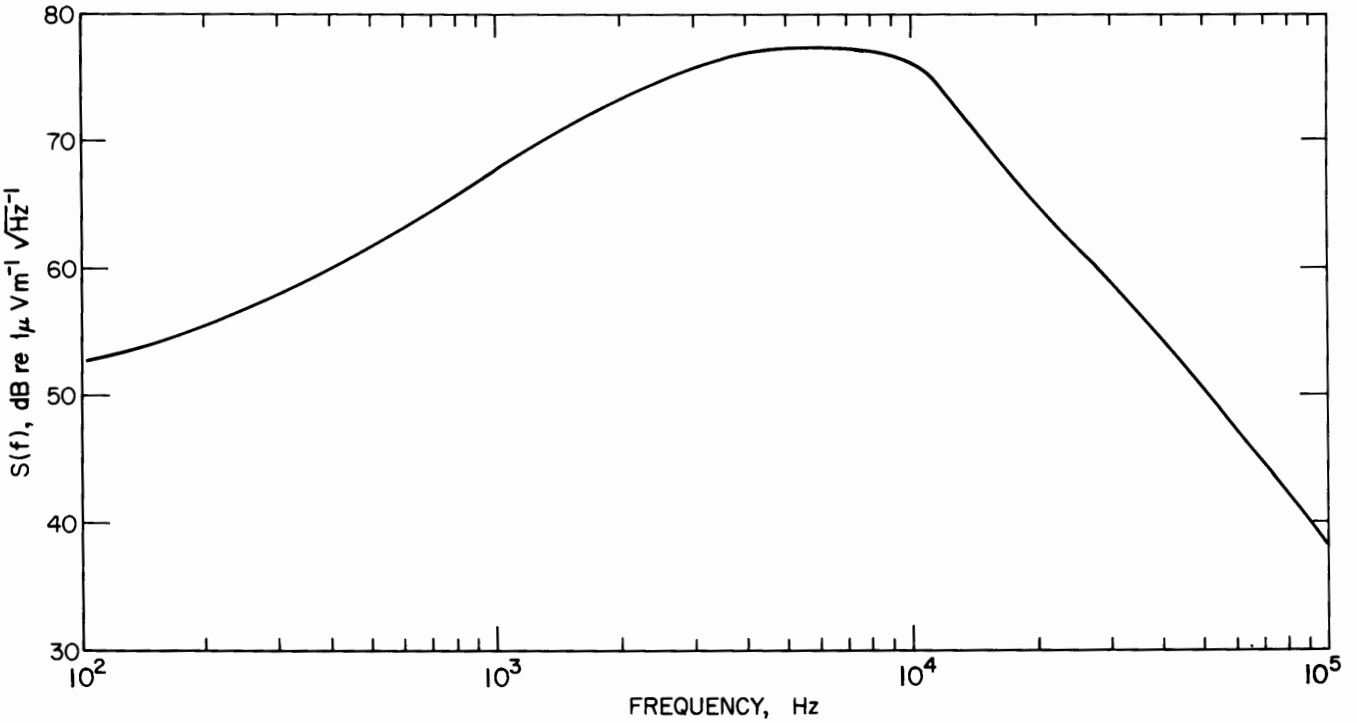

FIGURE 3. - Expected frequency spectrum of radiation component of electric field, normalized to a distance of 1 km (23).

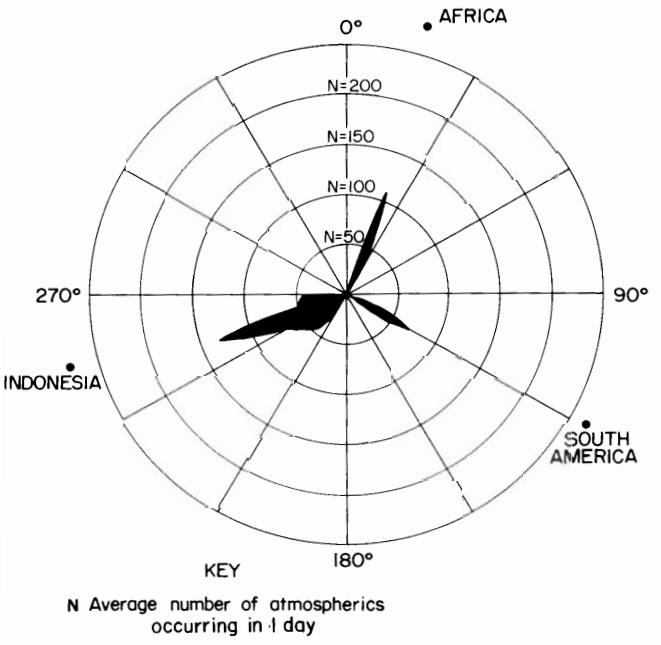

FIGURE 4. - Directionality diagram of average number of atmospherics occurring in 1 day (23).

EARTH-IONOSPHERE WAVEGUIDE

The noise from distant storms arrives at the observation point via the earth and ionosphere waveguide. How this waveguide influences the transmission of EM energy from distant storms has been studied by a number of investigators. A key exposition of this propagation mechanism was published by Wait (20). Wait pointed out that the earth and ionosphere act as a waveguide wherein radio energy propagates. Rappert (18) outlined a general theory of the propagation of ELF waves in the waveguide. Propagation occurs with a vertical electric field accompanied by a horizontal magnetic field. This mode of propagation is approximated by transverse electromagnetic (TEM) mode propagation between parallel conducting plates. However, energy losses in both the earth and the ionosphere cause bending or "tilt" of the wave front toward the lossy medium, and consequently, a horizontal electric

field is generated at the surface of the earth. The interaction of EM waves with the earth is the basis of the study of magnetolellurics.

The radiated electric field shown in equation 5 can be rewritten in a more common form when the source current is considered in the form of I exp ($i\omega t$) and the propagation delay times appear as phase shifts of the form

$$E_0 = i \frac{\eta}{\lambda} I h_e \frac{\exp^{-ikd}}{d}, \qquad (8)$$

where k = wave number.

Following Wait's work, the vertical electric and horizontal magnetic fields from a distant lightning stroke can be found from

$$E_z = W E_0 \qquad (9)$$

and

$$H_\phi = T E_0/\eta, \qquad (10)$$

where $\left(\frac{W}{T}\right) = \left(\frac{d/a}{\sin d/a}\right)^{1/2} \frac{(d/\lambda)^{1/2}}{(h/\lambda)}$

$$\exp [i(2\pi d/\lambda - \pi/4)].$$

$$\sum_{n=0}^{\infty} \delta_n \left(\frac{S_n^{3/2}}{S_n^{1/2}}\right) \exp (-i2\pi S_n d/\lambda). \qquad (11)$$

In these equations, λ = wavelength, km,

$d = 2\pi/\lambda$,

a = Earth's radius, km,

δ_n = mode excitation factor ($\delta_0 \sim 1/2$; $\delta_n \sim 1$, where n = 1, 2, 3...),

h = height of the ionosphere (70 to 90 km),

and S_n = complex parameter of mode n.

The terms W and T above represent the electric and magnetic transfer functions of the waveguide. Also, it is assumed that kd >> 1. The distance d should now be considered the arc length between the source and observer. The exponential term of equation 11 can be written as

$$\exp (-i2\pi S_n d/\lambda) = \exp (-\alpha_n - i\beta_n)d, \qquad (12)$$

where α_n, the mode decay factor, is equal to $\frac{2\pi f}{c} \mathrm{Im}(S_n)$,

in which Im = imaginary part;

and where β_n, the waveguide wave number, is equal to $\frac{2\pi f}{c} \mathrm{Re}(S_n)$,

in which Re = real part.

The units of α_n are nepers per unit of distance. If the unit of distance chosen is 1,000 km (1 Mm) then the attenuation can be expressed in decibels per megameter as

$$\overline{\alpha_n} = (20 \ \mathrm{LOG}_{10} e) \ \alpha_n \qquad (13)$$

or

$$\overline{\alpha_n} = 0.182 \ f \ \mathrm{Im}(S_n). \qquad (14)$$

S_n is obtained from the roots of a modal resonance equation. At ELF, and in many cases at VLF, the flat earth form of the equation

$$R_g R_i \exp [-2kh(1 - S_n^2)^{1/2}] - 1 = 0 \qquad (15)$$

is applicable. R_g and R_i are the planar complex reflection coefficients of the ground and ionosphere, respectively.

Barr (4) has computed the variation of $\overline{\alpha_n}$ with frequency for a realistic daytime ionosphere model. The results showed that for equal mode excitation factors, only the zero-order mode is significant in the ELF and lower VLF bands. Results for north-to-south propagation are shown in figure 5.

Experimental propagation studies have shown the earth-ionosphere waveguide to be anisotropic due to the earth's magnetic field. The greatest effect of the waveguide on propagation is at frequencies ranging from 1 to 4 kHz. For east-to-west propagation, the attenuation in

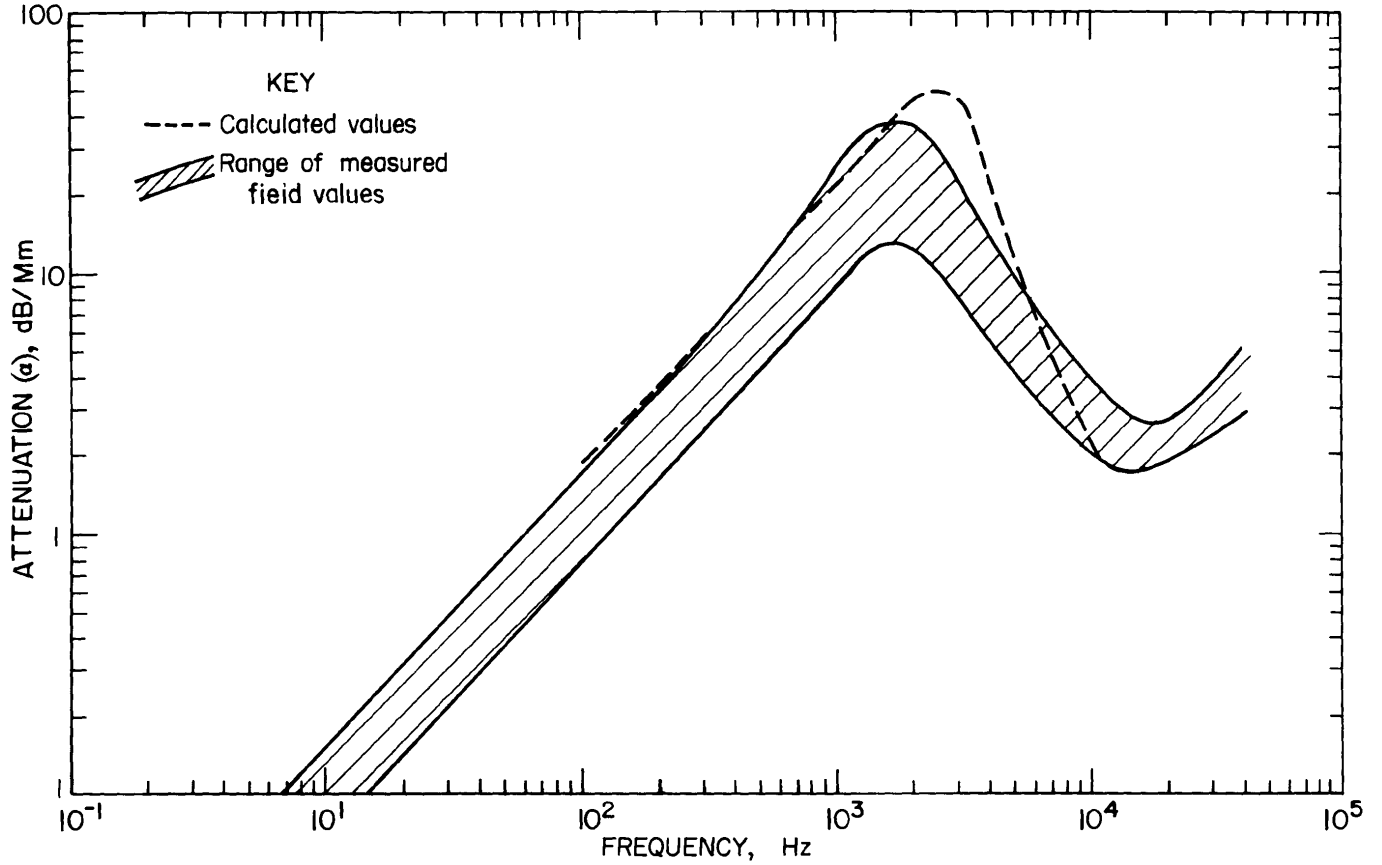

FIGURE 5. - Propagation attenuation coefficient of earth-ionosphere waveguide.

this frequency range is as much as 20 dB lower than the north-to-south curve of figure 5, while west-to-east propagation is as much as 30 dB greater than this curve.

Also shown in figure 5 is the range of coefficient values for propagation attenuation measured by different investigators. Below 10 kHz, the values are based on lightning spheric measurements by Jean (13), and Chapman (9) and on cavity resonance measurements by Balser (3). (Resonance effects are not shown.) Above 10 kHz, the values are based on work by Eckersly (10) and Pierce (17). Barr's theoretical frequency dependence of the attenuation of the earth-to-inosophere waveguide (4) agrees well with the measurements.

The magnitude of the electric field for the zero mode in the far zone can be written as

$$|E| = \frac{\eta\, Ih_e}{h[\lambda a \sin(d/a)]^{1/2}} \Lambda_0 \exp^{-\alpha_0 d}, \quad (16)$$

where the factors δ_0 and S_0 have been collected in a mode excitation factor Λ_0.

Considering the noise-source spectrum shown in figure 3, the relative expected vertical electric noise field spectrum, at a given observation point, would appear as shown in figure 6. Plotted in figure 6 are the relative spectra of the electric field as measured at different distances from the source. The null in the noise spectras appearing in the 2- to 3-kHz range is aligned with the peak of the channel attenuation spectrum of figure 5 and is consistent with the observations of many studies.

The observed magnetic noise spectra would be much like that of the electric spectra, but its amplitude would be smaller (1 to 3 dB) than the magnetic

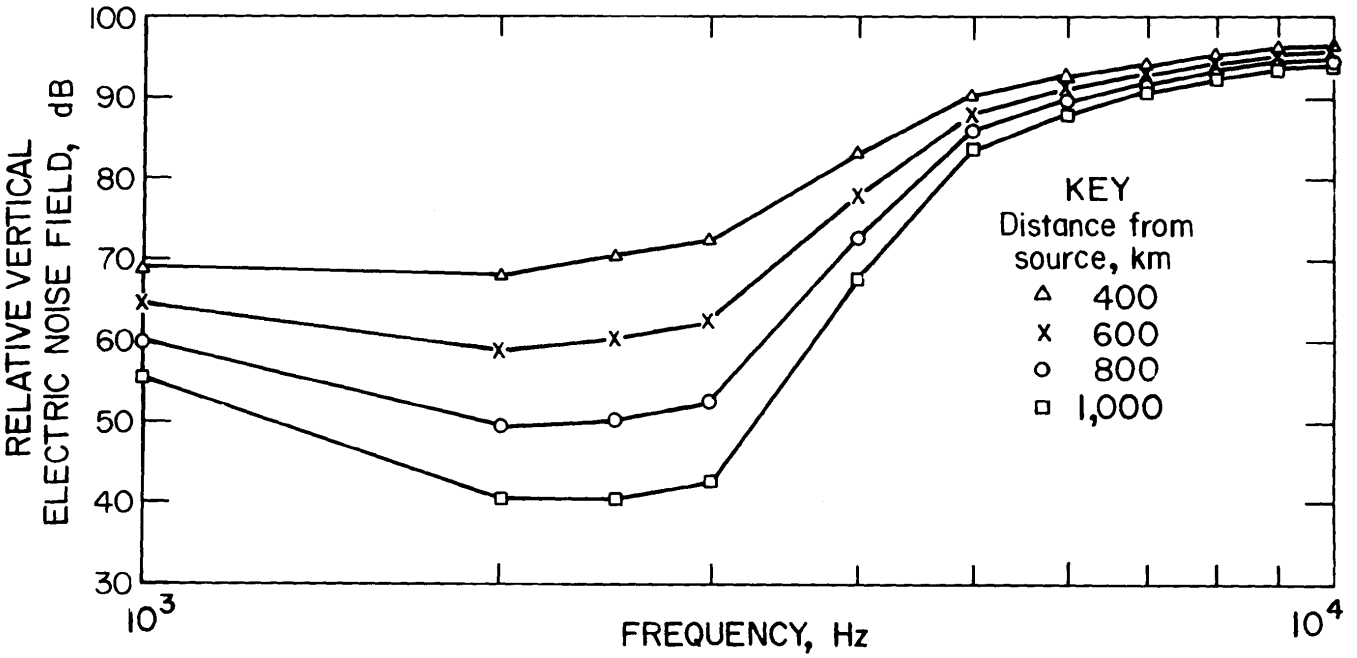

FIGURE 6. - Relative vertical electric noise field spectrum.

field calculated from the free space electric and magnetic wave impedance relationship. A smaller amplitude would be expected because of an increase in the wave impedance below 10 kHz. This increase is caused by waveguide attenuation and a phase velocity exceeding the speed of light above 1 kHz and below 10 kHz.

PRIOR ATMOSPHERIC NOISE MEASUREMENTS

For TTE communications, the range of frequencies of interest is approximately 200 Hz to 6 kHz. Thus both the ELF and VLF bands are included. Also, since communication may be uplink and downlink, both surface and subsurface noise must be considered. While atmospheric noise data are readily available for the frequency band between 10 kHz and 32 MHz, relatively few reported atmospheric noise measurements have been made below 10 kHz. For TTE communication between horizontal loops, the subject of this study, the interfering noise component comes from the vertical magnetic noise. However, of the few noise studies that have been done for frequencies below 10 kHz, most have been concerned with the vertical electric field strength or the horizontal magnetic field strength because of their applicability to surface-based, long-range radio communications.

Possibly the best reference on atmospheric radio noise is CCIR Report 322 (8). This report contains worldwide contour maps of atmospheric noise levels at 1 MHz for 4-h intervals for 3-month periods. With each map, curves of frequency dependence are given, but the lower limit of each curve is 10 kHz. Thus the results are not directly useful for baseband communications.

During the 1960's and the 1970's, because of the interest in long-distance communications to submarines, some atmospheric noise measurements were made in the ELF range. A special issue of the Institute of Electrical and Electronics Engineers (IEEE) "IEEE Transactions on Communications," (21), was devoted to ELF communications and Project Sanguine and contains several references to ELF noise. Soderberg (19) gives an extensive bibliography on ELF noise and lists presently active ground stations with capability for measuring ELF noise.

Vertical electric noise measurements were made over the frequency range of 1 Hz to 100 kHz by Maxwell and Stone (15). Some of their results are shown in figure 7 and are consistent in form with the theoretical curves shown in figure 6. Maxwell (14) made vertical electric atmospheric noise field measurements over a 2-year period at a number of worldwide locations for the frequency range of 20 Hz to 30 kHz. Average field measurements were obtained and amplitude probability distributions of the vertical electric field were derived. The amplitude probability distributions were also used to convert the average measurements to RMS values.

The National Bureau of Standards (NBS) made wideband noise measurements both within and above numerous coal mines (5-6). Most of these measurements were made while the mines were operating, and manmade 60-Hz harmonic noise was generally dominant. For rescue TTE communications, the mine power would be off, except for ventilation, therefore manmade noise should not be a factor. The main interference would be expected to come from atmospheric noise caused by worldwide thunderstorm activity.

Most published data of ELF or VLF atmospheric noise are either of the vertical electric field or the horizontal magnetic field because they are the dominant components of both the TEM and the first-order transverse magnetic (TM) modes in the earth-ionosphere waveguide. However, for loop-to-loop TTE communications, vertical magnetic noise is the source of interference.

SURFACE VERTICAL MAGNETIC NOISE

In most applications of EM communications, the vertical electric field is used, owing to the propagation characteristic of the earth-ionosphere waveguide. Therefore, noise measurements were made of the vertical electric field and/or horizontal magnetic field. When only one of these two fields was measured, the other was assumed to be related by the free space impedance (377 Ω), which would be in slight error as previously discussed.

NBS (1) measured both horizontal and vertical magnetic noise in a remote area of Utah with no power lines in the vicinity. The vertical component tended to be 10 to 15 dB below the horizontal

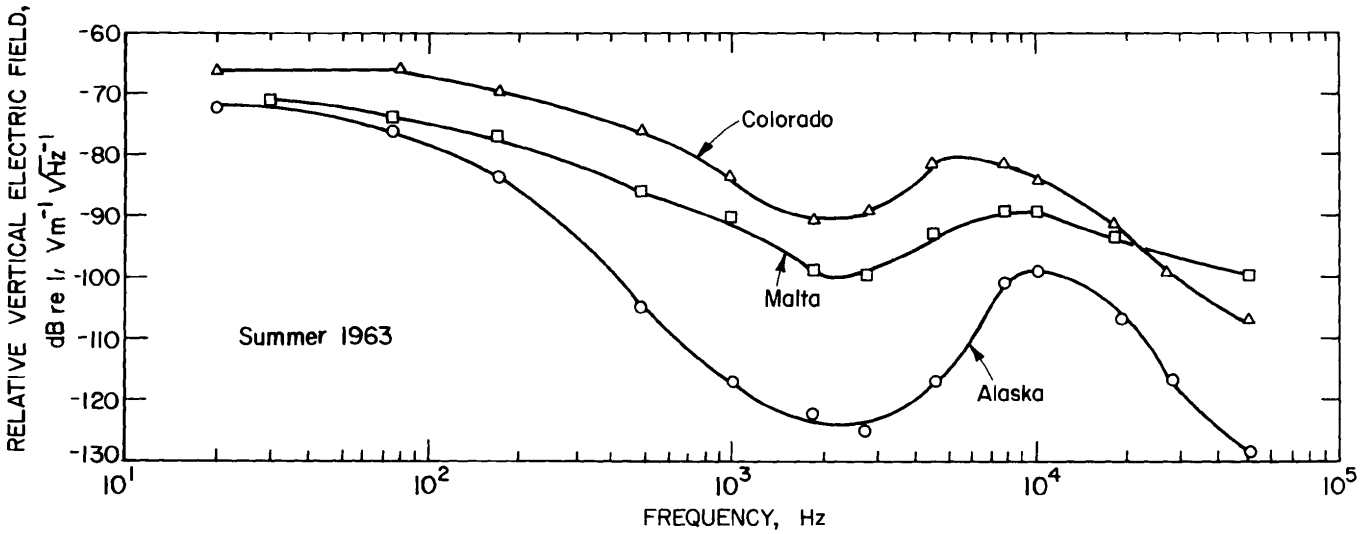

FIGURE 7. - Typical vertical electric field noise measurements (15).

component, which is consistent with earlier dip-angle measurements by Ward (22).

In geophysical prospecting, the magnetotelluric method is often used for locating underground ore bodies (24). This method uses the EM field from a thunderstorm to obtain information on the localized conductivity structure. This source field, as previously discussed, has a vertical electric field and a horizontal magnetic field. Over a homogeneous conducting earth, such an orientation would not produce a secondary field with a vertical magnetic field. Where a noise measurement is to be made, it is informative to study how the noise field from a distant storm may interact with the local earth conductivity structure to produce secondary fields that may give rise to a vertical magnetic component.

In the following discussion, it is assumed that at a given observation point the horizontal magnetic field is generated by independent distant thunderstorms (K) and that a given source (H_i) is located at azimuth angle ψ_i. Using a rectangular coordinate system, the horizontal magnetic field components can be resolved into x and y components as

$$H_x = - \sum_i H_i \sin \psi_i \qquad (17)$$

and

$$H_y = \sum_i H_i \cos \psi_i . \qquad (18)$$

The geometry of the situation is shown in figure 8. The tangential field components are continuous and, for the frequencies of interest, displacement currents can be neglected and the propagation constants (γ) in the air and earth respectively become

$$\gamma_o = i\omega (\mu_o \epsilon_o)^{1/2} \qquad (19)$$

and

$$\gamma_1 = (i\omega \mu_o \sigma_1)^{1/2}, \qquad (20)$$

where $|\gamma_o| << |\gamma_1|$.

Because of the relationship between the propagation constants, the direction of the wave at z = 0 into the earth can be approximated as parallel to the z-axis.

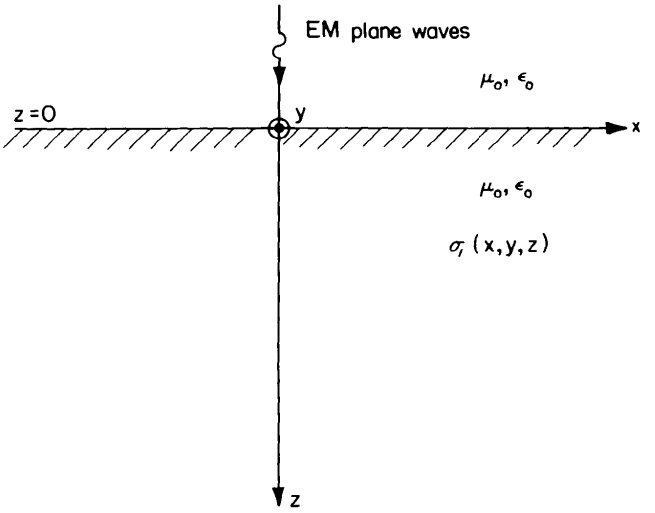

FIGURE 8. - Coordinate system and earth conductivity model.

This approximation allows the view that the incident field is also parallel to the z-axis in the limit as $z \to 0$. The primary H-field at the surface (H_p) can then be given as

$$H_p(z) = H_p \exp^{-\gamma_1 z} \qquad (21)$$

and

$$[H_p] = \begin{bmatrix} H_{px} \\ H_{py} \\ 0 \end{bmatrix}. \qquad (22)$$

The total H-field in the region above the earth is then a linear combination of the primary field and secondary field (H_s) caused by the conductivity structure of the earth and is given as

$$H(r) = H_p(r) + H_s(r), \qquad (23)$$

where r is some fixed location.

The secondary field in the earth can be related to the surface primary field (24) by

$$[H_s (r)] = [K_{mn}(r)] [H_p(0)], \qquad (24)$$

where

$$K_{mn}(r) = \sum_i \hat{K}_{mn_i} \left[\exp^{-\Gamma_i r} + R_{mn_i} \exp^{-\Gamma'_i r} \right],$$

in which $m \to x, y, z$,

$n \to x, y$,

R_{mn_i} → surface reflection coefficients from z > o side,

$$\Gamma_i = \bar{i}\,\gamma_{xi} + \bar{j}\,\gamma_{yi} + \bar{k}\,\gamma_{zi},$$

and $$\Gamma'_i = \bar{i}\,\gamma_{xi} + \bar{j}\,\gamma_{yi} - \bar{k}\,\gamma_{zi}.$$

At the surface, for z = o,

$$K_{mn}(x, y, o) \sum_i \hat{K}_{mn_i} \exp^{-\gamma_{x_i}x - \gamma_{y_i}y} \cdot(1 + R_{mn_i}). \quad (25)$$

Therefore, the contribution to the total surface horizontal magnetic field is based upon $R_{mn_i} \neq -1$. For the situation of a homogeneous earth, the primary H-field encounters no variation in the propagation medium for z > 0; and thus $R_{mn_i} = -1$, and no secondary magnetic fields exist. Likewise, for a one-dimensional earth with $\sigma_1 = \sigma_1(z)$, $K_{mn}(0) = 0$ for all m, n. For a three-dimensional earth, $\sigma_1 = \sigma_1(x, y, z)$; there can be reflected secondary waves at any angle, and a vertical H-field is created. In this case, K_{mn} can be treated as a random variable having any value.

Not only does this information show how a vertical magnetic field can be created, it also shows that the magnitude relationship between the horizontal and vertical fields is not clearly defined. In the literature, it is often stated that the vertical magnetic field is smaller than the horizontal field, but there is no guarantee of this. For example, as was shown in the "Noise Source" section, there appear to be three primary azimuth sectors in which most atmospherics occur (fig. 4). It is conceivable that the horizontal magnetic noise measurement could be aligned so as to minimize the response to these noise sources while the localized conductivity structure could give rise to large vertical fields.

Hill (12) has shown how a vertical magnetic noise field can be generated by three simple earth models. Hill derived equations for the vertical magnetic noise field for (1) a conducting earth model in which the earth is homogeneous but the air-earth interface is slightly rough, (2) an earth model consisting of a thin, laterally inhomogeneous conducting sheet at an arbitrary depth in an otherwise homogeneous half-space, and (3) a homogeneous earth model containing an infinitely long conducting cylinder representative of manmade object such as a wire, rail, or pipe or a natural object such as a long ore body. Hill's studies of each of these models showed how the vertical magnetic noise field is created and for particular parametric values showed the behavior of the field both in space and frequency.

UNDERGROUND VERTICAL MAGNETIC NOISE

Since downlink communication is impaired by underground EM noise, an understanding of the expected noise levels below the earth's surface must be obtained in order to evaluate TTE communications. Also, since the assumed method of communications is between horizontal loop antennas lying flat on the ground, vertical magnetic noise is the component of interest.

It can be assumed that during a mine emergency condition, the primary source of underground noise will be from the surface noise field. As previously discussed, due to the relative values of the propagation constants above and within the earth, the noise wave tends to propagate perpendicularly into the earth. Therefore, for a homogeneous earth, no underground vertical magnetic noise field would be expected; and as was the case for the surface, a vertical magnetic noise would occur underground only in the presence of spatial earth conductivity variations.

An interesting study of this problem was made by Hill (12). Hill modeled the earth as a homogeneous half-space

containing a laterally periodic thin sheet of high conductivity (fig. 9). The conductivity of the half-space is σ_o, and the conducting sheet, of thickness d, is located at a depth h. The sheet conductivity $\sigma(x)$ is periodic in form, as shown below.

$$\sigma(x) = \sigma + \Delta \cos \beta x, \qquad (26)$$

where $\beta = 2\pi/L$ and L,

in which L = the period. Using this earth model, Hill developed equations for the vertical magnetic field within the earth and found that it could be approximated as

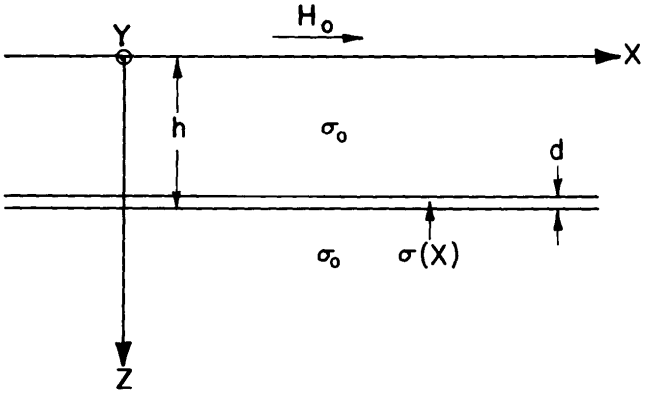

FIGURE 9. - Geometry of homogeneous half-space earth model with thin conducting sheet.

$$H_z \simeq \frac{\beta \Delta d \eta \, H_x \sin \beta x}{2\Gamma_1} \begin{cases} \dfrac{\cos(\Gamma_1 z)}{\cos(\Gamma_1 h)} \exp^{-\Gamma_1 h}, & o < z < h \\ \exp^{-\Gamma_1 z}, & z > h \end{cases}, \qquad (27)$$

where $\eta = \dfrac{i\omega\mu_o}{\gamma}$,

in which $\gamma = (i\omega\mu_o\sigma_o)^{1/2}$;

H_x = horizontal magnetic field at surface;

and $\Gamma_1 = (\gamma^2 + \beta^2)^{1/2}$.

The values for σd and $|\Gamma_1|h$ are assumed to be small. Also, since the earth's permeability is assumed to be that of free space, H_z at $z = 0$ is equal to the surface vertical magnetic noise field.

Equation 27 not only shows how a surface vertical magnetic field can be created due to lateral conductivity changes, it also shows both the depth and frequency dependence of the vertical magnetic field within the earth. Equation 27 also shows that as L becomes very large, $H_z \to 0$, which is consistent with earlier discussions of the absence of a vertical magnetic noise field for a conducting earth with no lateral conductivity changes. Also, if $|\beta/\gamma|$ is small, then the exponential term of equation 27 for the region of $z > h$ reduces to $\exp(-\gamma z)$, which is the traditional skin effect of a wave in a conducting media.

Hill's earth conductivity model was chosen for use in this study as an aid in predicting the behavior of the vertical magnetic noise within the earth. However, like any modeling attempt, its value depends upon its ability to explain trends in actual field data.

Due to the lack of sufficient data on vertical magnetic noise above and in coal mines, field tests were conducted at a number of coal mines throughout the United States to obtain recordings of this noise. The results are described in the following sections.

EM VERTICAL MAGNETIC NOISE FIELD TESTS

NOISE MEASURING INSTRUMENTATION

Noise recordings were made on-site and later reduced in the laboratory to obtain the desired noise information. Surface noise measurements were made at each mine, and when possible, in-mine noise measurements were made at the same time. A diagram of the instrumentation used is shown in figure 10.

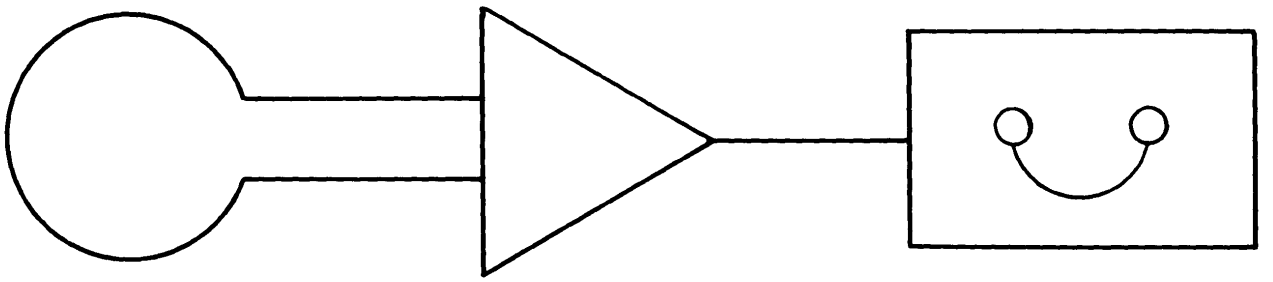

FIGURE 10. - Field test recording instrumentation.

The antenna used was a 15-in-diam loop of 500 turns of wire. During the tests this loop was laid flat on the ground. To relate the output voltage of the loop to a magnetic field of known frequency in which it was immersed, the loop was calibrated by a method described by Greene (11). The limit of uncertainity of this method is believed to be ±3 pct.

The amplifier used was a Princeton Applied Research[3] (PAR) model 113. This amplifier has variable gain and variable low-pass and high-pass filter settings. Its input noise voltage is -165 dB re 1.0 V-RMS $\sqrt{Hz}^{-1}$. The input current noise does not contribute significantly to the overall noise because of a low source impedance.

The tape recorder was a Nagra model IV-SJ. This tape recorder has variable attenuation but was maintained for one-to-one reproduction throughout the tests. The recorder's equivalent input noise voltage was found to be -127.8 dB re 1.0 V-RMS $\sqrt{Hz}^{-1}$.

The system noise included both the amplifier and tape recorder the input noise values and the amplifier gain setting. This system noise can be expressed as

$$V_N = [(5.75 \times 10^{-9} \times G)^2 + (4.07 \times 10^{-7})^2]^{1/2}, \quad (28)$$

where V_N = system noise voltage, V-RMS $\sqrt{Hz}^{-1}$

and G = amplifier gain.

V_N was constant over the frequency range of interest, and the corresponding system magnetic noise was found by referencing the loop calibration factor at the frequency of interest.

Several minutes of noise was recorded at each mine site, and attempts were made to obtain measurements both above and within each mine. All of the recordings were made during the afternoon hours over a period from March to November.

For reduction of the noise data, the tapes were played through the instrumentation diagramed in figure 11. The tape deck and amplifier were the same ones used during the field tests. A Krohn-Hite model 3500 bandpass filter was used to eliminate noise outside the band of interest. Noise amplitudes were obtained at discrete frequencies using a Nicolet Scientific model 444A fast Fourier transform (FFT).

[3]Reference to specific equipment or manufacturers does not imply endorsement by the Bureau of Mines.

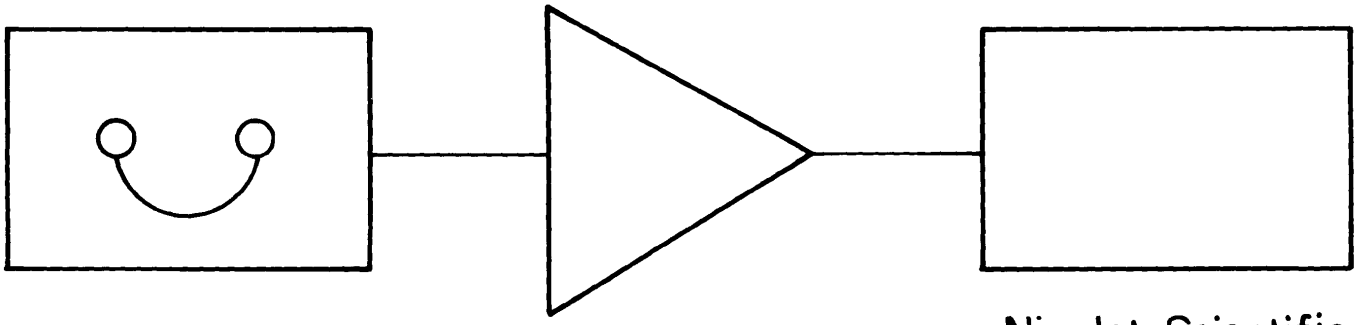

FIGURE 11. - Playback instrumentation.

NOISE DATA

For evaluating a noise communication system, the RMS value of the noise is the important factor to consider. The noise tapes were reduced by performing a high-resolution FFT (0.38 Hz noise equivalent bandwidth) on the data. Thirty-two independent samples of 4-s duration were averaged to obtain the average RMS voltage noise level at a particular frequency. This procedure was repeated to obtain the RMS voltage noise levels at a number of different frequencies. Using the calibration factor of the reproduction instrumentation (fig. 11), the field amplifier gain, and the calibration factor of the loop antenna, magnetic noise values were then obtained.

For each mine where noise was recorded, table 1 shows the surface noise field values in dB re 1.0 $\mu A\ m^{-1}\ \sqrt{Hz}^{-1}$ -RMS for different frequencies. Where possible, underground noise measurements were also made, using instrumentation similar to that used on the surface; these measurements are also shown in table 1, in the same units. (The mines listed by number in table 1 are identified by name and location in appendix C.) The surface and underground measurements were made simultaneously, and at all but four mines (mines 24, 25, 26, and 27), the data was obtained while the mine was operating. Both the surface and underground data exclude manmade 60-Hz harmonic noise, which is often much greater than the random background noise reported here.

As stated earlier, the system noise can be expected to change with the gain of the field amplifier. However, if the gain is large, the system noise can be attributed to the amplifier noise. This was the situation in the majority of the cases, and at no time were the data found to be system noise limited when the amplifier gain was low. Therefore, table 1 also includes the equivalent magnetic noise level of the field instrumentation.

Since the noise values were obtained by averaging a number (N = 32) of independent noise samples from a given tape, the statistical accuracy of the data must be considered. For an estimate of a spectral density function S(f) by way of an FFT method which calculates both the real and imaginary values of S(f), the degrees of freedom, df, are twice the number of samples obtained as explained by Otnes (16). Assuming that the samples were independent Gaussian variables with zero mean and unit variance, the summation of the square of the samples would be chi-square distributed. Therefore, the confidence interval of S(f) can be written as

$$\text{Prob}\ (A < S(f) < B) = p. \qquad (29)$$

TABLE 1. - Surface and underground vertical magnetic noise values obtained at different sites

(dB re 1.0 μA m^{-1} $\sqrt{Hz}^{-1}$)

	Frequency, Hz							
	270	630	1,050	1,950	2,490	3,030	4,530	5,970
SURFACE MEASUREMENTS								
Mine:								
1	-12.7	-22.6	-34.8	-42.3	-44.1	-47.4	-48.3	-52.7
2	-4.4	-19.5	-29.7	-34.0	-34.0	-36.4	-36.3	-42.7
3	-9.0	-24.6	-33.7	-40.0	-40.0	-44.5	-48.9	-49.4
4	7.7	-11.0	-21.3	-35.8	-35.8	-32.2	-38.4	-37.6
5	-15.3	-29.9	-36.0	-45.3	-45.3	-36.5	-55.8	-56.2
6	-14.2	-21.4	-28.5	-41.8	-41.8	-46.4	-51.1	-49.4
7	2.6	-7.1	-13.5	-31.1	-31.1	-37.6	-43.2	-46.0
8	9.9	-4.1	-15.3	-15.3	-15.3	-19.6	-29.0	-33.8
9	-3.4	-15.2	-20.3	-32.3	-32.3	-36.8	-34.6	-37.2
10	-1.9	-11.4	-22.4	-27.1	-29.7	-36.9	-43.5	-44.0
11	4.9	-9.5	-21.3	-32.7	-34.9	-38.2	-41.0	-49.4
12	4.9	-8.2	-14.7	-21.8	-22.6	-27.1	-30.3	-34.7
13	-.7	-13.6	-20.6	-26.2	-28.8	-29.0	-35.9	-42.3
14	11.4	.1	-7.5	-17.9	-20.7	-23.4	-23.8	-22.3
15	-9.3	-18.7	-23.4	-30.9	-32.6	-36.1	-38.3	-30.5
16	-17.0	-23.8	-34.0	-40.9	-48.0	-48.9	-51.0	-52.3
17	-21.8	-31.6	-38.3	-45.8	-45.8	-50.0	-53.8	-57.3
18	-.2	-16.6	-27.2	-34.7	-34.5	-37.3	-36.7	-34.7
19	-10.9	-20.5	-29.4	-41.0	-39.8	-49.2	-53.2	-56.4
20	17.4	.1	-8.2	-18.6	-25.0	-25.7	-30.2	-29.8
21	-9.6	-22.1	-30.0	-37.6	-37.8	-40.3	-36.5	-49.7
22	1.2	-11.5	-20.4	-21.9	-27.6	-31.4	-33.8	-41.4
23	-1.7	-18.1	-28.5	-36.0	-38.8	-41.9	-42.4	-45.5
24	-15.8	-29.3	-31.7	-45.0	-47.2	-50.8	-56.6	-58.4
25	3.0	-11.4	-19.5	-29.3	-29.9	-31.4	-27.1	-25.7
26	-19.0	-31.9	-39.8	-49.5	-51.8	-54.6	-60.3	-61.8
27	-14.4	-30.8	-37.7	-49.3	-51.0	-55.1	-58.6	-59.5
System noise	-28.6	-36.0	-40.5	-46.4	-48.9	-51.0	-56.9	-64.0
UNDERGROUND MEASUREMENTS								
4	ND	-14.2	-22.4	-27.5	-30.8	-33.4	-36.1	-39.9
10	ND	-32.1	-31.6	-44.1	-46.3	-51.5	-54.7	-57.8
16	ND	-23.3	-30.1	-35.6	-37.2	-39.4	-39.1	-44.6
18	ND	-23.1	-27.4	-37.7	-40.2	-42.9	-49.3	-52.2
24	ND	-28.7	-36.3	-45.5	-47.7	-50.5	-55.5	-63.6
25	ND	-11.9	-25.9	-35.6	-38.6	-41.9	-46.6	-46.7
26	ND	-32.5	-40.7	-48.6	-51.0	-54.4	-58.5	-60.6
27	ND	-30.8	-34.8	-44.7	-47.1	-51.6	-56.1	-56.9
28	ND	-20.4	-28.0	-35.3	-35.0	-41.8	-41.8	-42.2
System noise	NAp	-36.0	-40.5	-46.4	-48.9	-56.9	-56.9	-64.0

ND Not detected. NAp Not applicable.

The parameter p is a fixed confidence level. A related parameter, α, is often referred to with

$$\alpha = 1 - p. \tag{30}$$

The confidence limits A and B can then be written as

$$A = \frac{df\ \hat{S}(f)}{\chi^2_{df,\alpha/2}} \tag{31}$$

and

$$B = \frac{df\ \hat{S}(f)}{\chi^2_{df,\ 1-\alpha/2}}. \tag{32}$$

For the FFT sampling performed on the noise data, df = 64. Therefore, a 95-pct confidence interval on the noise data is

$$\frac{64}{88}\hat{S}(f) < \hat{S}(f) < \frac{64}{44}S(f)$$

or -2.3 to 3.3 dB. These accuracy figures should represent the accuracy of the noise measurements since the error of the data-gathering and reduction instrumentation is much lower than these figures.

DATA ANALYSIS

The purpose of this study was to gain an understanding of noise, both on the earth's surface and underground, that would degrade TTE communications. It is expected that underground noise would be less than surface noise due to the conducting earth which separates the surface from underground locations. Unfortunately, in the majority of the cases, the data were obtained while the mine was operating, meaning that the data may have been influenced by the mine machinery. Analysis of the data should therefore result in a conservative estimate of the expected natural noise present. Where the underground noise was greater than the surface noise, the underground data were probably mostly influenced by the operating mine. This occurred for mines 4 and 16 (table 1). Therefore, the underground noise data for these two mines were disregarded.

Expected noise levels were derived by statistical inference, using noise models generated from the surface and underground data. A corollary objective of the analysis was to understand the interrelationships of the surface and underground noise.

For the purpose of evaluating a communication system, the most important relationship to determine is that of the expected noise level at a given frequency. Table 2 shows the mean and standard deviation noise values for both the surface and underground noise measured at the mines listed in table 1 and appendix C. Also shown in table 2 is the difference, in decibels, between the surface and underground mean noise values. (The mean decibel difference values are included only to show that expected noise values are lower for the underground locations. These values do not represent expected differences at a given mine since the surface data set was for a larger number of mines than the underground data set.)

TABLE 2. - Surafce and underground vertical magnetic noise mean and standard deviation values

($\mu A\ m^{-1}\ \sqrt{Hz}^{-1}$)

	Frequency, Hz							
	270	603	1,050	1,950	2,490	3,030	4,530	5,970
Surface:								
Mean.....	1.165	0.235	0.090	0.035	0.027	0.020	0.014	0.013
Standard deviation.....	1.562	.266	.105	.043	.028	.024	.015	.017
Underground:								
Mean.....	ND	.078	.030	.010	.008	.005	.003	.003
Standard deviation.....	ND	.081	.014	.005	.005	.004	.002	.002
Mean differential.....dB..	ND	-9	-9	-11	-11	-12	-13	-14

ND No data collected.

In agreement with prior atmospheric noise studies, the mean noise values in table 2 decrease as frequency increases. However, no indication of a noise null, which has been reported by others, is present in the average data. Likewise, in almost all of the individual mine surface noise data shown in table 1, no noise null is evident. Possibly the explanation for this has to do with the frequency-dependent earth reflection coefficients discussed earlier, but additional studies would need to be performed to confirm this. Also, since most of the tests were performed while the mine was operating, the surface measurements may have been influenced by underground mine impulsive noise.

The mean noise values are plotted in figure 12. It can be seen that the surface vertical magnetic noise values obtained at the mines are in the same range as the horizontal magnetic noise values found by Maxwell (15) (fig. 7).

In evaluating the performance of a communication system, it is valuable to have a statistical model of the noise so that probability statements can be made about the expected value of the noise at a given frequency. A common method used

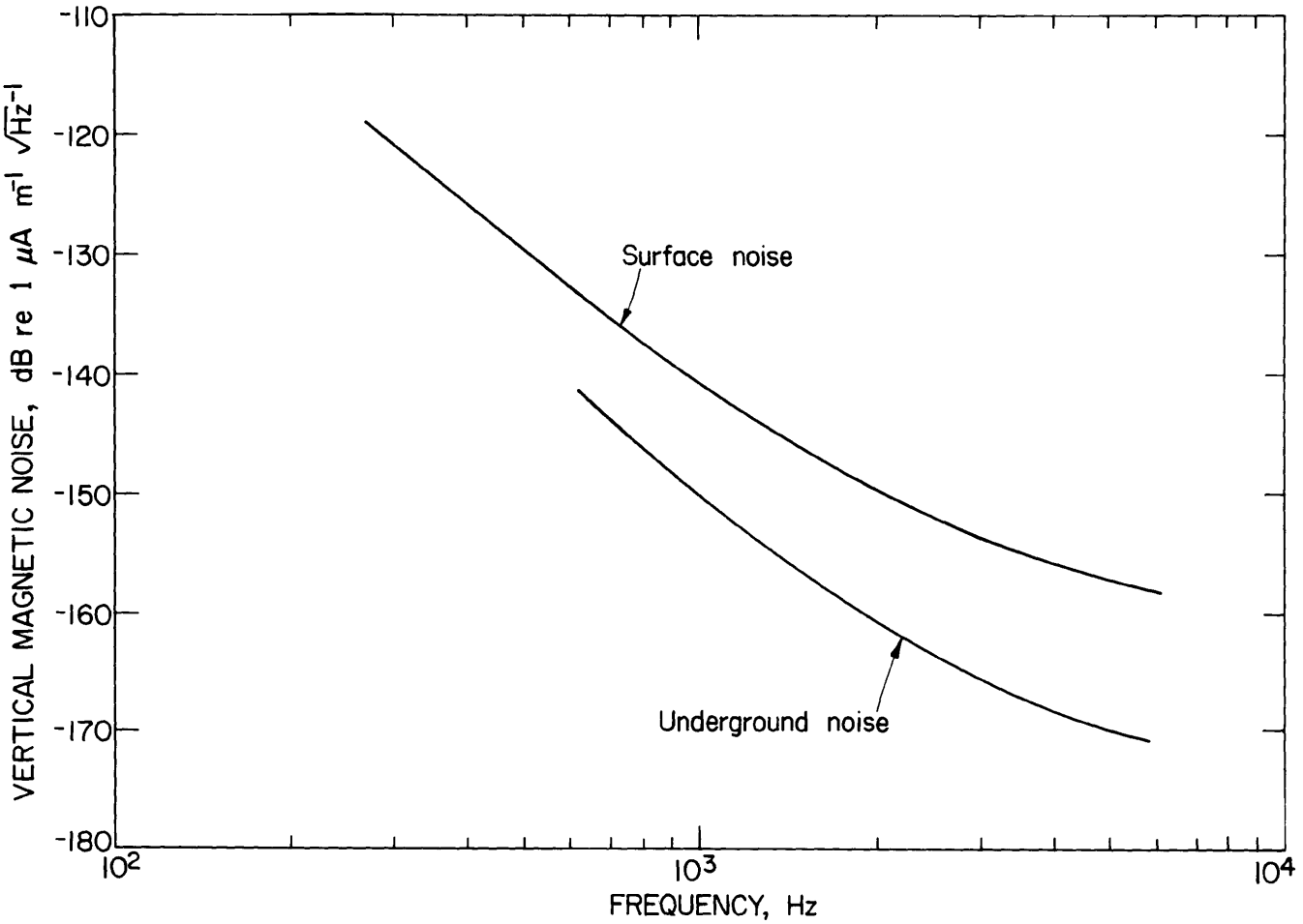

FIGURE 12. - Surface and underground mean vertical magnetic noise values from noise data.

to achieve this is through regression analysis.

Several linear regression models were hypothesized and tried. The model found to best fit the behavior of the data is one in which the mean value of the noise level H_N is linearly related to the logarithm of the frequency. This is shown by

$$H_N = \alpha + \beta_i \log (f_i) + \varepsilon. \quad (33)$$

H_N is the vertical magnetic noise level, expressed in dB re 1 $\mu A\ m^{-1}\ \sqrt{Hz}^{-1}$. The parameters α and β_i are parameters to be estimated from the data. The parameter ε represents a random variable that is normally distributed, with expected value zero and a variance which is the same for all values of i.

The derived regression lines for both the surface and underground noise are shown in figure 13, and the regression results are summarized in table 3. The correlation coefficients given in table 3 (for the regression results of both the surface and underground noise) are large enough to assume that the linear regression models are reasonably acceptable.

It was assumed that the errors were normally distributed and that the variance was equal across the independent variable. These assumptions were considered and it was concluded that meaningful statistical inferences from the regression analysis could be made.

Also shown in figure 13 are bands around the regression lines which represent intervals of confidence; within these intervals, one can be 95-pct confident that the expected mean relationship between noise and frequency actually exists. Such an interval is commonly referred to as a confidence interval (CI). The CI is found from

$$H_{Nj} = T_{\alpha/2,df}\ s_{yx} \left[\frac{1}{n} + \frac{(F_j - \bar{F})^2}{S_{xx}} \right]^{1/2}, \quad (34)$$

where $T_{\alpha/2,df}$ is a statistical value based on sampling distribution theory, in which

α = 5 pct

and $df = n - 2$,

and where n = number of samples,

F_j = the particular frequency value,

$\bar{F}$ = average value of frequency tested,

s_{yx} = standard error of the estimate of the regression relationship,

and $S_{xx} = n - 1\ (s_x)^2$,

where S_{xx} is the corrected sum of squares for frequency and is the estimate of the standard deviation of the frequency tested.

From figure 13 it can be seen that the vertical distance between the upper and lower band of each of the two confidence

TABLE 3. - Regression results for vertical magnetic noise (dB re 1.0 $\mu A\ m^{-1}\ \sqrt{Hz}^{-1}$ vs LOG (frequency))

	Surface noise	Underground noise
Number of observations...	216	49
Estimated intercept.....	67.09	58.72
Estimated slope.....	-30.15	-30.03
Correlation coefficient..	.80	.87
Estimated standard error.	9.79	5.46
Standard deviation of log frequency.....	.43	.32

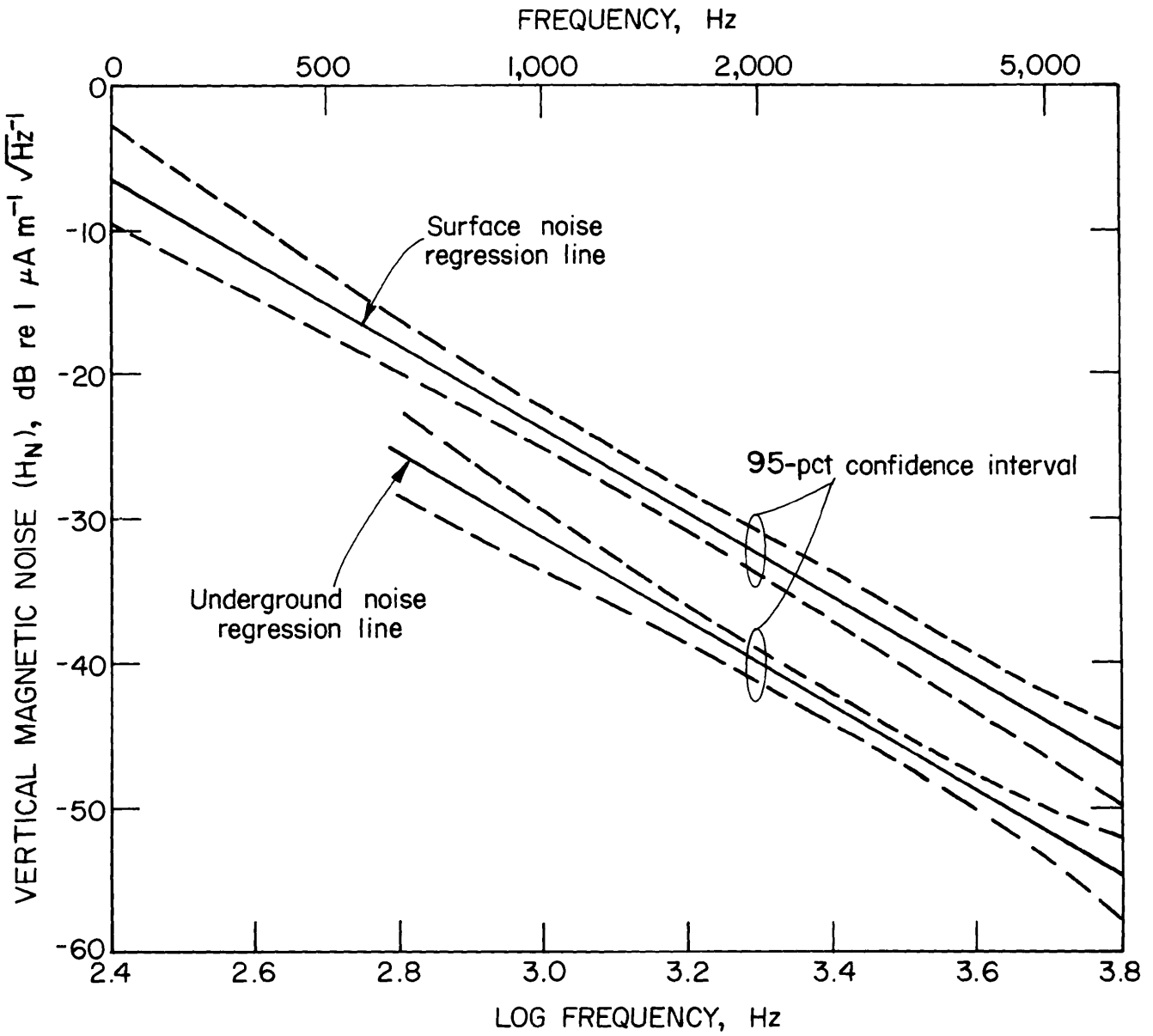

FIGURE 13. - Regression results for surface and underground vertical magnetic noise versus frequency.

intervals is smallest at $F_j = \bar{F}$ and that this distance becomes greater the further F_j is from $\bar{F}$. This means that less trustworthy information exists about the relationship between noise and frequency at the smaller and larger frequencies; the regression line is more reliable for at those frequencies in the middle range.

Figure 13 also shows that the expected underground noise levels are lower than the expected surface noise levels. This would be anticipated if the only source of the underground noise were the surface noise. However, the expected underground noise levels may be questionable since system noise problems were encountered in measuring the noise in mines 24, 25 and 27. Nonetheless, even though the data from these three mines may not represent the true noise levels, the information gathered remains valuable because it is known that the true noise levels are lower than the system noise. The

underground noise regression model could be used in evaluating downlink communications and would lead to conservative estimates of performance.

The regression lines in figure 13 provide information on the expected level of the vertical magnetic noise at a given frequency. In the evaluation of a communication system, estimates of expected performance during times of high or low noise are also of value. Considering the standard error estimates of table 3, a reasonable assumption of the range of surface noise values would be that of the surface regression line, ±10 dB. Likewise, for the underground noise values, the range of noise variation would be approximately ±5 dB around the underground regression line.

A common method used in estimating the expected speech intelligibility of a communciation system is known as the articulation index (AI) (2). When the AI method is used, the noise is generally measured in one-third octaves. The expected noise levels derived from this study are shown in one-third octaves, for both the surface and underground, table 4.

Though the regression models shown in figure 13 might be used in making probability statements on expected surface and underground noise levels, the results should not be interpreted as establishing a relationship between surface and underground noise. This is because the surface noise measurements were drawn from a much larger data base than the underground measurements were.

To obtain information on the surface and underground noise relationship, a subgroup of data would need to be taken from both the surface and underground data base which contained results from the same mines. In addition, data for such a study should not be thermal noise limited. Once the subgroup of data was obtained, a 2-parameter linear regression model might be found that would relate the difference in surface and underground noise to mine depth and frequency. Unfortunately, the only subgroup of data of this kind from this study contained only three mines, mines 10, 18, and 25. Meaningful statistical inferences would be difficult to make using such a small set of data.

As discussed earlier in the section, "Underground Vertical Magnetic Noise," Hill (12) estimated the expected variation of the underground vertical magnetic field for a homogeneous earth model containing a highly conductive thin sheet.

TABLE 4. - Expected vertical magnetic noise values for one-third octaves

Band	Center frequency, Hz	Bandwidth, Hz	Noise, dB re 1.0 μA m^{-1}	
			Surface	Underground
1.....	200	44	14.1	6.1
2.....	250	56	12.3	4.2
3.....	315	75	10.5	2.4
4.....	400	95	8.4	.4
5.....	500	110	6.1	-1.9
6.....	630	150	4.5	-3.6
7.....	800	190	2.3	-5.7
8.....	1,000	220	.1	-7.9
9.....	1,250	280	-1.8	-9.8
10.....	1,600	400	-3.5	-11.5
11.....	2,000	440	-6.0	-14.0
12.....	2,500	560	-7.9	-15.8
13.....	3,150	750	-9.6	-17.6
14.....	4,000	950	-11.7	-19.7
15.....	5,000	1,100	-14.0	-21.9

It would be valuable to obtain additional data on both surface and underground vertical noise to establish the appropriateness of this model.

SUMMARY

For evaluating the performance of a through-the-earth voice communication system which uses horizontal antennas, information on the expected levels of vertical magnetic noise both on the surface and underground is needed. The source of this noise and its propagation to an observation point was discussed. The interaction of this propagating noise field with the localized conductivity structure was also discussed as it lates to the formation of a vertical magnetic field and its variation underground. Surface and underground vertical magnetic noise measurements were made at a number of different mines from which statistical models that relate the expected noise level as a function of frequency were derived. The results were also presented in one-third octaves, which allows evaluation of the expected performance of a communication system to be accomplished through a method known as the articulation index.

REFERENCES

1. Adams, J. W., W. D. Bensema, and N. C. Tomoeda. Surface Magnetic Field Noise Measurements at Geneva Mine. NBS, Boulder, CO, Rep. 74-369, June 1974, 35 pp.

2. American National Standards Institute. Methods for the Calculation of the Articulation Index. ANSI 53.5-1969, 1969, p. 24.

3. Balser, M., and C. A. Wagner. Observations of Earth-Ionosphere Cavity Resonances. Nature, v. 188, June 1960, pp. 638-644.

4. Barr, R. The Propagation of ELF and VLF Radio Waves Beneath an Inhomogeneous Anisotropic Ionosphere. J. Atmos. and Terr. Phys., v. 33, 1971, pp. 343-353.

5. Bensema, W. D. Coal Mine ELF Electromagnetic Noise Measurements. NBS, Boulder, CO, Rep. 10-739, Apr. 1972, 90 pp.

6. _____. A Noise Spectum Measurement System Using the Fast Fourier Transform. IEEE Trans. Electromagn. Compat., v. EMC-19, Apr. 1977, pp. 37-43.

7. Bradley, P. A., and F. Homer. The Spectra of Lightning Discharge at Very Low Frequencies, J. Atmos. Terr. Phys., v. 26, 1964, pp. 1069-1073.

8. CCIR (International Radio Consultative Committee). World Distribution and Characteristics of Atmospheric Radio Noise. Rep. 322, Int. Telecommun. Union, Geneva, 1965, p. 78.

9. Chapman, F. W., and R. V. Macario. Propagation of Audio Frequency Radio Waves to Great Distances. Nature, v. 177, May 1956, pp. 930-933.

10. Eckersley, T. L. Studies in Radio Transmission. J. IEEE, v. 27, Sept. 1932, pp. 405-459.

11. Greene, F. M. NBS Field-Strength Standards and Measurements (30 Hz to 1000 MHz). Proc. IEEE, v. 55, No. 6, June 1967, pp. 970-981.

12. Hill, D. A., and J. R. Wait. Theoretical Noise and Propagation Models for Through-the-Earth Communication. BuMines contract J0113058, unpublished report, 1982, 45 pp; available for consultation from Harry Dobroski at Pittsburgh Res. Center, BuMines, Pittsburgh, PA.

13. Jean, A. G., J. R. Wait, and D. F. Wasmundt. Observed Attenuation Rate of

ELF Radio Waves. J. Res. NBS, Sect. D, v. 65D, Sept.-Oct. 1961, pp. 475-479.

14. Maxwell, E. L. Atmospheric Noise from 20 Hz to 30 kHz. Radio Sci., v. 1, No. 6, July 1967, pp. 637-644.

15. Maxwell, E. L., and D. L. Stone. Natural Noise Fields From 1 cps to 100 Kc". IEEE Trans. Antennas and Propag., v. Z, 1963, pp. 339-343.

16. Otnes, R. K., and L. Enochson. Applied Time Series Analysis. V. 1, Basic Techniques. Wiley 1978, 449 pp.

17. Pierce, J. A. Sky-Wave Field Intensity. I. Low and Very Low Radio Frequencies. Cruft Lab., Harvard Univ., Cambridge, MA, Tech. Rep. 158, 1952, 12 pp.

18. Roppert, R. A., and W. F. Moler. Propagation Theory and Calculations at Lower Extremely Low Frequencies (ELF). IEEE Trans. Comm., v. COM-22, No. 4, Apr. 1974, pp. 438-451.

19. Soderberg, E. G. ELF Noise Surveys, A Review. NATO/AGARD Meeting of Electromagnetic Wave Propagation Panel, Brussels, Belgium, Sept. 21-25, 1981, 11 pp.

20. Wait, J. R. Electromagnetic Waves in a Stratified Media. Pergamon, 1962, 372 pp.

21. _____. Special Issues on ELF Communication. IEEE Trans. Comm., v. COM-22, No. 4, Apr. 1974, pp. 353-538.

22. Ward, S. H., J. O'Donnel, R. Rivera, G. W. Wave, and D. C. Fraser. AFMAG-Applications and Limitations. Geophysics., v. 31, 1966, pp. 576-605.

23. Watt, A. D. VLF Radio Engineering. Pergamon, 1967, 703 pp.

24. Word, D. R., H. W. Smith, and F. X. Bostic. An Investigation of the Magnetotelluric Tensor Impedance Method. Electrical Geophysics Res. Lab., Univ. of TX, Austin, TX, Tech. Rep. 82, March 1970, 264 pp.

APPENDIX A.--ABBREVIATIONS AND SYMBOLS USED IN THIS REPORT

NOTE.--This list does not include (1) the unit of measure abbreviations listed at the front of this report, (2) most abbreviations and symbols that are identified and then used only briefly in a single place within the report, and (3) the abbreviations and symbols used in (and identified in) appendix B.

a	Earth's radius
AI	articulation index
c	velocity of light
CI	confidence interval
CW	continuous wave
d	distance
df	degrees of freedom
E_z	vertical electric field
ELF	extremely low frequency
EM	electromagnetic
f	frequency
FFT	fast Fourier transform
G	gain
h_e	effective height of lightning stroke
H_i	thunderstorm noise source
H_N	vertical magnetic noise level
H_ϕ	tangential magnetic field
i	imaginary number
I	current
IEEE	Institute of Electrical and Electronic Engineers
Im	imaginary part
k	planewave number
K	distant thunderstorms
L	period
M	lightning stroke charge moment
N	noise measurement
NBS	National Bureau of Standards
q	charge
R	correlation coefficient
R_{mn}	reflection coefficient
re	relative
Re	real part
RMS	root mean square
S(f)	noise source spectral density function
t	time
T	magnetic field ionosphere waveguide transfer function
TEM	transverse electromagnetic
TM	transverse magnetic
TTE	through the earth
V_N	system noise voltage
VLF	very low frequency
W	electric field ionosphere waveguide transfer function
α_n	mode decay factor
β_n	waveguide wave number
Γ	vector propagation constant
γ	propagation constant
σ_n	mode excitation factor (Λ is also used for this term.)
ε	permittivity
η	free-space wave impedance
θ	angle (ϕ is also used for this term.)
Λ	mode excitation factor (σ_n is also used for this term.)
λ	wavelength
μ	permeability
σ	conductivity
τ	waveform duration
ϕ	angle (θ is also used for this term.)
Ψ	angle of arrival

APPENDIX B.--INSTRUMENTATION NOISE

There are universal noise models for any two-port network. The network is considered as a noise-free black box, and the internal sources of noise are represented by a pair of noise generators located at one port, usually the input.

The receiving antenna for this study is assumed to be a multiturn loop deployed in a circle. At lower frequencies, stray capacitance may be ignored, and the loop antenna may be represented by an inductance in series with a resistance. This receiving loop, coupled with a receiver preamplifier, is shown in figure B-1.

The amplifier noise voltage (E_{na}) is represented by a zero-impedance voltage generator in series with the input port. The amplifier noise current (I_{na}) is given as an infinite-impedance current generator in parallel with the input. Both of these generators may be frequency dependent. The antenna signal and noise voltages may also be frequency dependent. The source resistor noise is Johnson noise and is given as

$$E_{ns}^2 = 4KTRB, \qquad \text{(B-1)}$$

where K = Boltzmann's constant (1.38×10^{-23} J/K),

T = temperature, K,

and B = bandwidth, Hz.

This noise is independent of frequency. All of these generators may be assumed to be independent of each other. Also, it is assumed that $R_{IN} >> R$ and $R_{IN} >> X_L$ (inductor reactance).

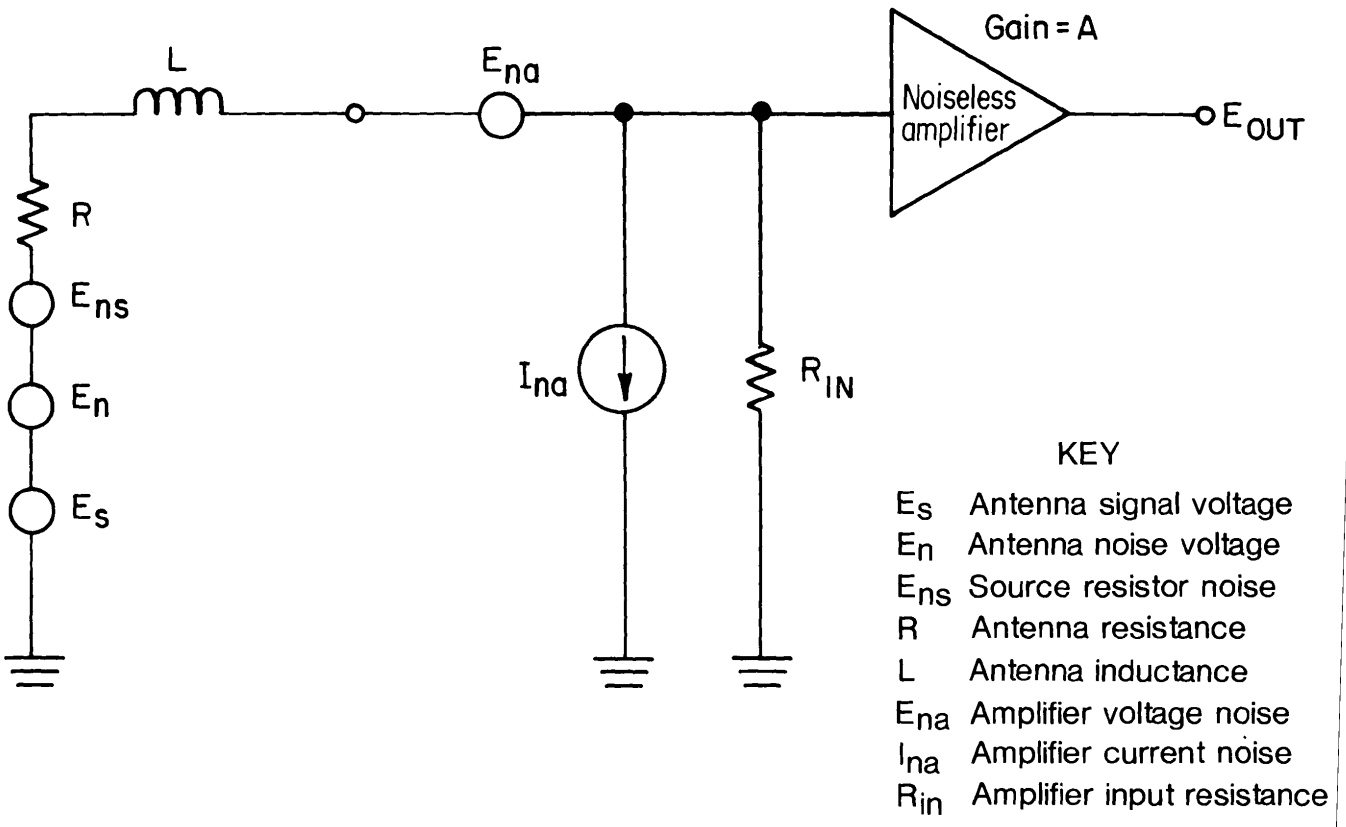

FIGURE B-1. - Noise-equivalent model of receiver.

In choosing an amplifier to couple with a sensor, a conventional method is to choose one that has a low noise figure (NF). While NF valves are useful for comparing amplifiers, they are not necessarily appropriate indicators for optimizing the noise performance of an amplifier circuit. That is, the highest signal-to-noise ratio (SNR) may not be obtained under the same circuit conditions which minimize the NF.

In determining the NF, E_n is assumed zero. The NF is defined as

$$NF = 10 \text{ LOG} \left[\frac{\text{Input power SNR (amplifier disconnected)}}{\text{Amplifier output power SNR}} \right]$$

$$= 10 \text{ LOG } K^*. \qquad \text{(B-2)}$$

For the case of figure B-1, K* is found as follows:

$$K^* = \frac{E_{na}^2 + I_{na}^2 Z_s^2 + 4KTRB}{4KTRB}, \qquad \text{(B-3)}$$

where Z_s is the source impedance and the output SNR_O is given as

$$SNR_O = \frac{E_s^2}{E_n^2 + 4KTRB + E_{na}^2 + I_{na}^2 Z_s^2}. \qquad \text{(B-4)}$$

Therefore, for a given amplifier, the SNR is maximized when R = 0, but this sets the NF to infinity. For a given source impedance, the least noisy amplifier is the one with the smallest NF.

In many applications, the source and amplifier impedances are given, and the task is to match these in some manner to provide the maximum SNR. This matching can be found by setting

$$\frac{dK^*}{dZ_s} = 0. \qquad \text{(B-5)}$$

From this it is found that

$$Z_{opt} = E_{na}/I_{na}, \qquad \text{(B-6)}$$

the value Z_{opt} being the optimum source impedance. To obtain Z_{opt}, transformer of proper turns ratio (α), is used to couple the source to the amplifier such that

$$\alpha^2 = E_{na}/I_{na}Z_s. \qquad \text{(B-7)}$$

The transformer will perform best when working with a given source and fier; however, it is an additional component which in itself may be noisy. Therefore, before one uses a transformer, it must be determined whether the potential improvement will provide an actual one. This determination can only be made by investigating the nature of the signal source. Obviously, if the antenna noise voltage (which is caused by EM noise) is very high, this will be the limiting factor in performance, and no gain will be obtained through matching. In fact, this is the situation desired. The performance of the receiver should be determined by the external noise and not by the instrumentation.

To determine the limitations that the receiver amplifier could potentialy place on the system performance, the nature of the receiver antenna must be studied. The induced voltage (V) in a multiturn air-core loop antenna is given by

$$V = 2\pi f N A \mu_o H, \qquad \text{(B-8)}$$

where f = frequency, Hz,

N = number of turns in the loop,

A = loop area, m^2,

μ_o = permeability of free space,

and H = field strength, A/m.

For the antenna impedance value of interest in this study and the typical range of I_{na} values the amplifier current noise source can be neglected. Therefore, SNR_o becomes

$$SNR_o = \frac{E_s^2}{E_n^2 + 4KTRB + E_{na}^2}, \qquad \text{(B-9)}$$

where $E_s^2 = (7.89\ fNA \times 10^{-6}\ H_s)^2$ (V^2/Hz),

$E_n^2 = (7.89\ fNA \times 10^{-6}\ H_n)^2$ (V^2/Hz),

and $B = 1$ Hz.

H_s and H_n are the corresponding signal and noise field values at frequency f.

The resistance of the antenna can be expressed in terms of A as

$$R = 3.54\ (A)^{1/2}\ R_w\ N, \qquad \text{(B-10)}$$

where R_w = resistance per unit length of wire.

To prevent thermal noise limiting it is necessary that

$$E_n^2 > 4KTR + E_{na}^2 \qquad \text{(B-11)}$$

or that

$$(7.89\ f\ A \times 10^{-6}\ H_n)^2$$

$$> 4KT\ 3.54\ \sqrt{A}\ R_w\ N + E_{na}^2. \qquad \text{(B-12)}$$

This relationship can be used for determining the sensitivity of an air-core loop antenna amplifier arrangement or can be used for improving its sensitivity.

APPENDIX C.--MINE IDENTIFICATION

TABLE C-1. - Mines from which magnetic noise measurements were obtained

(All mines listed are coal mines.)

Mine	Depth, ft	Ownership	Mine name	Location	
				City	County and State
1.....	470	Youghiogheny & Ohio Coal Co.	Allison.....	Beallsville....	Belmont, OH.
2.....	58	Peabody Coal Co.	Alston No. 4....	Centertown.....	Ohio, KY.
3.....	1,550	Jim Walter Resources.	Blue Creek No. 3	Adger.....	Jefferson, AL.
4.....	381	Cal Glo.....	No. 21.....	Silver.....	Knox, KY.
5.....	400	Eastover Mining Co.	Highsplint No. 4	Highsplint.....	Hrlan, KY.
6.....	915	U.S. Steel.....	Gary No. 2	Wilcoe.....	McDowell, WV.
7.....	430	...do.....	Gary No. 9	Filbert.....	Do.
8.....	658	Gateway Coal Co.	Gateway.....	Clarksville....	Green, PA.
9.....	420	Allied Chemical Corp.	Harewood.....	Boomer.....	Fayette, WV.
10....	650	Alabama By-Products Corp.	Mary Lee No. 1..	Goodsprings....	Walker, AL.
11....	289	Monterey Coal Co.	Monterey No. 1..	Carlinville....	Macoupin, IL.
12....	540	Youghiogheny & Ohio Coal Co.	Nelms No. 2.....	Hopedale.....	Harrison, OH.
13....	560	Consolidation Coal Co.	Oak Park No. 7..	Cadiz.....	Do.
14....	650	Old Ben Coal Co.	Old Ben No. 26..	Sesser.....	Franklin, IL.
15....	70	Owl Creek Corp.	Sue-Jan.....	St. Charles....	Hopkins, KY.
16....	260	Peter Cave.....	No. 1.....	Lovely.....	Martin, KY.
17....	1,200	Plateau Mining Co.	Star Point No. 2	Wattis.....	Carbon, UT.
18....	500	Pontika.....	No. 1.....	Lovely.....	Martin, KY.
19....	600	North American Coal Co.	Powhatan No. 1..	Powhatan Point.	Delmont, OH.
20....	500	...do.....	Powhatan No. 3..	...do.....	Do.
21....	260	Peabody Coal Co.	Sinclair No. 2..	Drakesboro.....	Butler, KY.
22....	1,200	Kaiser Steel....	Sunnyside No. 2.	Sunnyside.....	Carbon, UT.
23....	460	Ziegler Coal Co.	Mine No. 4.....	Johnston City..	Williamson, IL.
24....	720	Helen Mining Co.	Helen.....	Homer City.....	Indiana, PA.
25....	282	Bureau of Mines.	Lake Lynn.....	Fairchance.....	Fayette, PA.
26....	220	([1]).....	J-4 Cave.....	University Park	Centre, PA.
27....	150	([1]).....	Woodward Cave...	...do.....	Do.
28....	388	Sewell Coal Co..	Meadow No. 1....	Lookout.....	Fayette, WV.

[1]On publicly owned property.

INT.-BU.OF MINES,PGH.,PA. 27205